Vibrational Spectroscopy of N_3^- in the Gas- and Condensed-Phase

Seyedeh Maryam Salehi, Debasish Koner, and Markus Meuwly*

Department of Chemistry, University of Basel, Klingelbergstrasse 80 , CH-4056 Basel, Switzerland.

E-mail: m.meuwly@unibas.ch

March 1, 2019

Abstract

Azido-derivatized amino acids are potentially useful, positionally resolved spectroscopic probes for studying the structural dynamics of proteins and macromolecules in solution. To this end a computational model for the vibrational modes of N_3^- based on accurate electronic structure calculations and a reproducing kernel Hilbert space representation of the potential energy surface for the internal degrees of freedom is developed. Fully dimensional quantum bound state calculations find the antisymmetric stretch vibration at 1974 cm^{-1} compared with 1986 cm^{-1} from experiment. This mode shifts by 64 cm^{-1} (from the frequency distribution) and 74 cm^{-1} (from the IR-lineshape) to the blue, respectively, compared with 61 cm^{-1} from experiment for N_3^- in water. The decay time of the frequency fluctuation correlation function is 1.1 ps, in good agreement with experiment (1.2 to 1.3 ps) and the full width at half maximum of the asymmetric stretch in solution is 18.5 cm^{-1} compared with 25.2 cm^{-1} from experiment. A computationally more efficient analysis based on instantaneous normal modes is shown to provide comparable, albeit somewhat less quantitative results compared to solving the 3-dimensional Schrödinger equation for the fundamental vibrations.

Introduction

Characterizing the structural and functional dynamics of complex systems in the condensed phase is a challenging problem, spanning several spatial and temporal scales.[1] One particularly elegant way to quantitatively assess the structure and dynamics of the solvent environment surrounding a probe molecule is to use optical spectroscopy, especially 1- and 2-dimensional infrared (1D-IR, 2D-IR) spectroscopy.[2] Two-dimensional IR spectroscopy is a powerful method for measuring the subpicosecond to picosecond dynamics in condensed-phase systems and considerably extends the toolbox of optical spectroscopy.

Using 2D-IR spectroscopy, the coupling between inter- and intramolecular degrees of freedom such as the hydrogen bonding network in solution, or structural features of biological macromolecules can be investigated by monitoring the fluctuation of fundamental vibrational frequencies of a probe molecule or ligand attached to a complex or a biological macromolecule. For quite some time, the amide-I stretching frequency has been used for this and has provided fundamental, molecular-level insight into the structural dynamics of small molecules and proteins alike.[3,4] For example, the CO chromophore was used as a probe to investigate the solvation dynamics of N-Methylacetamide in water.[3,5–10] Similarly, the CN^- stretching frequency has been used as a probe to investigate its own solvation dynamics[11–14] and structural and energetic features of a protein-ligand complex by attaching the probe to benzene.[15,16]

A versatile, spatially sensitive spectroscopic probe can also report on the dynamics of a system while minimizing the perturbations induced. The fundamental modes of a triatomic ligand such as the azide ion (N_3^-) are weakly coupled to the molecular framework it is bound to and can act as a sensitive probe for the environmental dynamics. The asymmetric stretching mode of N_3^- has a large oscillator strength and a vibrational transition frequency well separated from most organic chromophores. This makes it an ideal spectroscopic probe.[17–24] Other triatomic anions such as SCN^-, NCS^- or OCN^- have also served as spectroscopic probes.[25,26]

For a quantitative molecular level description of the environmental dynamics, a high-quality potential energy surface (PES) for the internal vibrational dynamics of the probe is required. Typically, differences of a few cm^{-1} are found when immersing the same probe into two different electrostatic environments, e.g. within a wild type and a single mutant protein.[15,16] Here, we use a combination of normal mode and numerically exact bound state calculations together with MD simulations in the gas- and condensed phase to characterize the vibra-

tional dynamics of N_3^- with the aim to provide the basis for its use as a covalently linked, positionally sensitive spectroscopic probe. The instantaneous deviation in the solute-solvent interactions is reflected by the fluctuation in the transition frequency of the fundamental modes. The time scale of the structural changes around the solute molecule can be determined from the decay of the frequency fluctuation correlation function (FFCF) from which also the lineshape of the 1D-IR spectrum can be obtained.[4]

The vibrational dynamics of N_3^- in the gas phase and solution has been investigated from experiment and computation. Experimentally, the NN asymmetric stretching frequency of the azide ion was determined to be at 1986.47 and 2047.5 cm^{-1} in the gas phase and bulk water, respectively[20,27,28] which make it a potentially useful environmental probe for protein dynamics, see Figure S1. Using non-linear infrared spectroscopy vibrational lifetimes of the asymmetric stretch fundamental of azide anion in water have been measured experimentally to be $T \approx 1.2$ ps (in H_2O)[29] and $T = 1.3$ ps (in D_2O).[18] The band width of the N_3^- asymmetric stretch in bulk water is 25.2 cm^{-1}.[20,29] Due to the triple bond character of azide,[30] its structure would stabilize through interaction with the solvent which leads to a blue shift (61 cm^{-1}) compared to the gas phase frequency.

Recently, an explicitly parametrized PES was computed using an accurate composite method based on pointwise, individually scaled fc-CCSD(T*)-F12b calculations including scalar relativistic effects and the aug-cc-pV5Z basis set. Using this PES, variational calculations determined the lower bound states for N_3^- in the gas phase with spectroscopic accuracy.[31] However, such a composite method is not feasible for the ultimate purpose of the present development, which is an accurate representation of the inter- and intramolecular interactions for N_3^- as a spectroscopic probe covalently linked to another molecular building block. In order to 1) accurately capture the energetics of distorted N_3^- geometries away from the equilibrium structure and 2) to cover situations in which the probe (N_3^-) and the moiety it

is linked to (e.g. an amino acid or a small organic molecule) are coupled electronically, it was decided to compute the PES at the multi reference CI (MRCI) level of theory. This also allows to extend the grid to a range that covers geometries further away from the equilibrium to sample conformations in MD simulations in sterically demanding environments due to local interactions and constraining effects.

In an effort to quantitatively capture the environmental dynamics, the present work introduces a computational model for the azido group capable of describing the molecular vibrations of the probe in gas- and the condensed-phase in a realistic manner. To this end, an accurate intramolecular, fully dimensional PES for N_3^- is computed based on high-level electronic structure calculations and represented as a reproducing kernel Hilbert space (RKHS). The vibrational transition frequencies of the fundamental modes are calculated from instantaneous normal mode (INM) analysis and from solutions of the nuclear Schrödinger equation. Results from bound state calculations including the vibrational line shapes from frequency correlation functions and the time scales for the environmental dynamics derived from them are then compared with data from experiments in the gas- and condensed phase.

First, the computational methods are presented. This is followed by quantum bound state and wave packet calculations to determine the stationary states for the low lying bound states. Next, the solvation dynamics in water is considered and the 1D-IR and the frequency fluctuation correlation functions, which are directly related to 2D-IR spectroscopy, are determined and discussed.

Methods

The Potential Energy Surface for N_3^-

The *ab initio* energies were computed at the multi reference configuration interaction (MRCI) level of theory including the Davidson correction (MRCI+Q) with the augmented Dunning type correlation consistent polarized quadruple zeta (aug-cc-pVQZ) basis set using the Molpro software.[32,33] All calculations were carried out for the $^1A'$ electronic state in C_s symmetry. Initial orbitals for the MRCI calculations were computed using the state averaged complete active space self-consistent field (SA-CASSCF) method for the first two $^1A'$ states with 16 electrons in 12 active orbitals and the $1s$ orbitals of the nitrogen atoms were kept frozen.

The *ab initio* energies were calculated in Jacobi coordinates (R, r, θ) (see the inset in Figure 1), where r is the distance between the two nitrogen atoms (N1 and N2), R is the distance between their center of mass and the third N atom (N3), and θ is the angle between $\vec{r}$ and $\vec{R}$. Evaluation of the necessary integrals in the bound state calculations (see below) is stablest and can be efficiently done if Gauss-Legendre points are used for the angular degrees of freedom.[34] Therefore, the angular grid (θ) used here contains 10 Gauss-Legendre quadrature points between 0 and 90° (6.721, 15.427, 24.184, 32.953, 41.726, 50.502, 59.278, 68.056, 76.833 and 85.611°) considering the symmetry of the system. The radial grids include 17 points along r ranging from 0.80 to 1.60 Å and 14 points along R between 1.38 and 2.14 Å.

For the bound state calculations and the molecular dynamics (MD) simulations in the gas phase and in solution a continuous and differentiable representation of the *ab initio* energies is required. Here, a reproducing kernel Hilbert space based approach[35,36] is used. A RKHS interpolation exactly reproduces a set of known function values and provides approximate values of the function at points where the values are unknown.

For the 1-dimensional kernels the linear problem $f(x_i) = \sum_j \alpha_j k(x_i, x_j)$ is solved which yields the coefficients α_j from which the value of the function $f(x) = \sum_i \alpha_i k(x_i, x)$ can be obtained for arbitrary x. The 3-dimensional kernel $K(X, X^{'})$ is then a tensor product of three 1-dimensional kernels.[36,37]

Based on this, the 3-dimensional kernel K is

$$K(X, X') = k^{(n,m)}(R, R')k^{(n,m)}(r, r')k^{(2)}(z, z'). \tag{1}$$

where X stands for all dimensions involved and

$$z = \frac{1 - \cos(\theta)}{2}, \tag{2}$$

which maps the angle θ onto the interval $[0, 1]$. The reciprocal power decay kernel ($k^{(n,m)}$) with smoothness $n = 2$ and asymptotic decay $m = 6$ is used for the radial dimensions (i.e., r and R)

$$k^{(2,6)}(x, x') = \frac{1}{14}\frac{1}{x_>^7} - \frac{1}{18}\frac{x_<}{x_>^8}, \tag{3}$$

where $x_>$ and $x_<$ are the larger and smaller values of x and x', respectively. For the angular degree of freedom, a Taylor spline kernel is used

$$k^2(z, z') = 1 + z_< z_> + 2z_<^2 z_> - \frac{2}{3}z_<^3, \tag{4}$$

where $z_>$ and $z_<$ are similar to $x_>$ and $x_<$.

Quantum Bound State Calculations

For solving the 3-dimensional Schrödinger equation of N_3^-, the DVR3D[38] software was used. DVR3D employs a discrete variable representation (DVR) based on Gauss-Laguerre quadratures for the radial and Gauss-Legendre quadratures for angular coordinates and thus yields a fully point-wise representation of the wave function. Solution of the vibrational problem is based on successive diagonalisation and truncation which is possible for a number of possible coordinate systems. After solving the vibrational bound state problem using DVR3D the wave functions and expectation values are obtained. The wave functions are then inspected to assign the quantum numbers of the vibrational states. For using the RKHS PES, an interface between DVR3D and the RKHS kernel code[36] was written. This code handles the transformations between the coordinates in which the PES is expressed and the coordinates employed by DVR3D.

Here, homonuclear Jacobi coordinates are employed because the PES is expressed in this coordinate system and the necessary angular integrals can be done efficiently and accurately using Gauss-Legendre quadrature. However, the problem can also be solved using other coordinate systems, e.g. bond-length bond-angle or Radau coordinates (ideal for heavy-light-heavy systems).[39] Ultimately, the choice of coordinate system primarily affects the rate of convergence of the eigenvalues which is relevant for highly excited states, but less so for the fundamentals considered in the present work. Here, the initial wave function is described by Morse oscillator functions for the radial coordinates. Several tests were carried out to converge the results by varying different parameters. The radial grid along r is defined by 40 points from 0.830 to 1.361 Å (1.57 to 2.57 a_0) using $r_e = 1.111$ Å (2.1 a_0), $D_e = 125.5$ kcal/mol (0.2 E_h) and $\omega_e = 3512$ cm^{-1} (0.016 E_h). For R, the grid is expanded from 1.409 to 2.106 Å (2.66 to 3.98 a_0) with 64 points and values of $r_e = 1.773$ Å (3.35 a_0), $D_e = 163.2$ kcal/mol (0.26 E_h) and $\omega_e = 2634$ cm^{-1} (0.012 E_h), respectively. For θ, 56 Gauss-Legendre quadrature points were used. Maximum dimensions of the intermediate 2D Hamiltonian and

the final Hamiltonian were 800 and 1200. For rotationally excited ($J > 0$) state calculations the $z-$axis was placed along $\vec{R}$.

To cross-validate the results from DVR3D, the Schrödinger equation for N_3^- was also solved for $J = 0$ following a time dependent wave packet approach.[40] Within this methodology, an initial wave packet $|\psi(0)\rangle$ is propagated using the split operator[41] method, followed by Fourier transformation of the autocorrelation function $\langle\psi(0)|\psi(t)\rangle$ and multiplied by an appropriate window function to obtain the energy spectrum. The radial grids were defined by 192 and 102 evenly spaced points for R and r, covering a range from 0.794 to 5.847 Å and from 0.529 to 3.736 Å, respectively. The angular grid consisted also of 56 Gauss-Legendre quadrature points. The initial wave packet was placed at $R = 1.781$ Å and $r = 1.188$ Å with widths of 0.106 and 0.079 Å along R and r, respectively, and was propagated for 80000 time steps with a time step of 8.0 a.u. ($\Delta t = 0.145$ fs). A Gaussian window function was used to obtain smooth and well resolved spectra.

Molecular Dynamics Simulations

For the MD simulations of N_3^- in solution, CHARMM[42] was used. Again, an interface between CHARMM and the multidimensional RKHS code was written for this. For the simulations in water the TIP3P[43] model was used (Figure 1). The nonbonded interactions were treated with a 12 Å cutoff switched at 8 Å. All bonds involving hydrogen atoms are constrained using SHAKE[44] as is also typically done for simulating proteins and polypeptides in solution.

Simulations of N_3^- in water were carried out in a pre-equilibrated cubic box of size 30^3 Å^3. First, the system was minimized using 2000 steps of steepest descent (SD) and 200 steps of Newton Raphson (ABNR) followed by 20 ps of heating to 300 K and 3.5 ns of equilibration

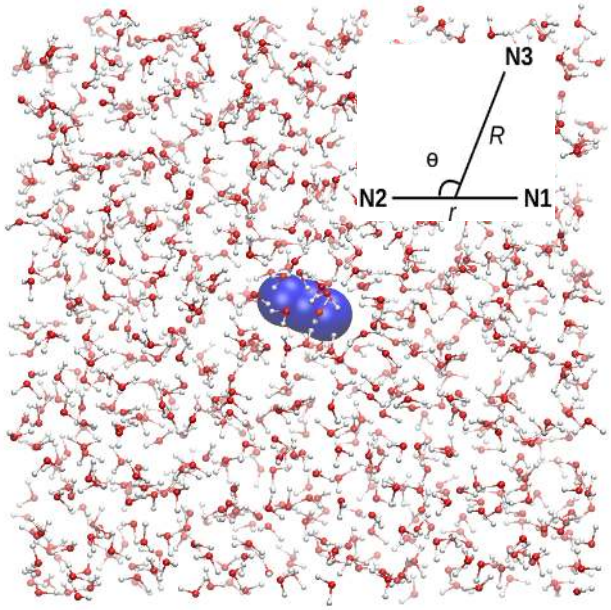

Figure 1: The simulation system used in the present work. N_3^- is displayed as blue van der Waals spheres and water molecules are shown as red (O atom) and white (H atom) ball and stick representation. The inset shows the Jacobi coordinates which define the *ab initio* energy grid.

MD at 300 K. Production simulations 8 ns in length were run in the NVE ensemble using the velocity Verlet integrator. The time step was $\Delta t = 1$ fs and snapshots for analysis were recorded every 5 time steps. Energy conservation for the present RKHS-implementation is reported in Figure S2 and is shown to be identical to the one for simulations without the solute.

For simulations in the condensed phase, nonbonded parameters for the N_3^- solute are required. The Lennard-Jones parameters for the nitrogen atoms were $\epsilon = 0.08485$ kcal/mol and $R_{\min}/2 = 1.66$ Å.[45] Charges are calculated following the Mulliken population analysis from the density matrix obtained at the MRCI/aug-cc-pVQZ level of theory. This yields a charge of $-0.53462e$ for the terminal nitrogen atoms and $0.06924e$ for the central one. As an extension, multipolar representations of the electrostatics could also be considered although

for closed-shell systems (e.g. N-methyl-acetamide) it has been found that point charge models can be quite reliable for spectroscopic[46] and thermodynamic[47,48] properties.

From the production simulation, 1.2×10^6 snapshots are taken as a time-ordered series for computing the frequency fluctuation correlation function and the 1D-IR spectrum. The FFCF was determined from either instantaneous harmonic vibrational frequencies based on a normal mode analysis or by using anharmonic frequencies calculated from solving the 3-dimensional nuclear Schrödinger equation using DVR3D. Normal modes of N_3^- were calculated for each snapshot after minimizing N_3^- and keeping the central N atom and the surrounding solvent frozen. Thus frequency trajectories were obtained for ω_1, ω_2 and ω_3 which correspond to the symmetric stretch, the bending and the asymmetric stretch vibration, respectively. The anharmonic transition frequencies ν_i were calculated using DVR3D calculations based on a 3-dimensional PES for N_3^- generated at each snapshot. To compute the 3D PES, the grid was defined in internal coordinates ($R_{\mathrm{N1-N2}}, R_{\mathrm{N2-N3}}, \angle N1N2N3$) by fixing the position of the central nitrogen, N2, and all water molecules. The grid consists of 15 points along $R_{\mathrm{N1-N2}}$ and $R_{\mathrm{N2-N3}}$ from 0.82 to 1.35 Å and 7 points for $\angle N1N2N3$ between 155° to 180° (158.490, 161.675, 164.859, 168.043, 171.225, 174.402 and 177.561°). The total energies were then calculated using the CHARMM+RKHS-module to obtain an analytical (RKHS) 3D PES for each snapshot. Finally, the ν_i were determined by solving the 3D Schrödinger equation for bound states using DVR3D as discussed before based on the 3D RKHS PES.

From the frequency trajectory $\omega_i(t)$ (or $\nu_i(t)$; all expressions below pertain to anharmonic frequencies in a similar fashion) of a particular mode i, its frequency fluctuation correlation function, $\langle \delta\omega(0)\delta\omega(t)\rangle$ is computed. Here, $\delta\omega(t) = \omega(t) - \langle\omega(t)\rangle$ and $\langle\omega(t)\rangle$ is the ensemble average of the transition frequency. From the FFCF the line shape function is determined

within the cumulant approximation

$$g(t) = \int_0^t \int_0^{\tau'} \langle \delta\omega(\tau'')\delta\omega(0)\rangle d\tau'' d\tau'. \tag{5}$$

To compute the line shape function $g(t)$, the FFCF is fitted to a general expression[49]

$$\langle \delta\omega(t)\delta\omega(0)\rangle = a_1 \cos(\gamma t) e^{-t/\tau_1} + \sum_{i=2}^{n} a_i e^{-t/\tau_i} + \Delta_0 \tag{6}$$

where a_i, τ_i, γ and Δ_0 are fitting parameters. The parametrization of this fitting function is motivated by the overall shape of the FFCF[49] and has been used in previous work.[14,50] It is an extension of the typical multiexponential decay, which is traditionally employed,[18] in order to capture the anticorrelation at short times. Furthermore, this functional form also allows analytic integration[4] to obtain $g(t)$ in Eq. 5. The decay times τ_i of the frequency fluctuation correlation function reflect the characteristic time-scale of the solvent fluctuations to which the solute degrees of freedom are coupled.

The 1D-IR spectra is then calculated as[20]

$$I(\omega) = 2\Re \int_0^\infty e^{i(\omega - \langle\omega\rangle)t} e^{-g(t)} e^{-\frac{t}{2T_1}} e^{-2D_{\mathrm{OR}}t} dt, \tag{7}$$

where $\langle\omega\rangle$ is the average transition frequency obtained from the distribution, T_1 (0.8 ± 0.1 ps) is the vibrational relaxation time and $D_{\mathrm{OR}} = 1/6T_R$ with $T_R = 1.3 \pm 0.3$ ps is the rotational diffusion coefficient which account for lifetime broadening.[19]

Results

Analytical Potential Energy Surface

The analytical PES for N_3^- was constructed from 2231 *ab initio* energies using a RKHS. To test its quality, an additional 245 *ab initio* energies are computed at off-grid points (which were not used in the RKHS interpolation) and are compared with the energies obtained from the RKHS PES, see Figure 2. The correlation coefficient between the *ab initio* and analytical energies is $R^2 = 0.9999$ which confirms the high quality and interpolative power of the RKHS PES.

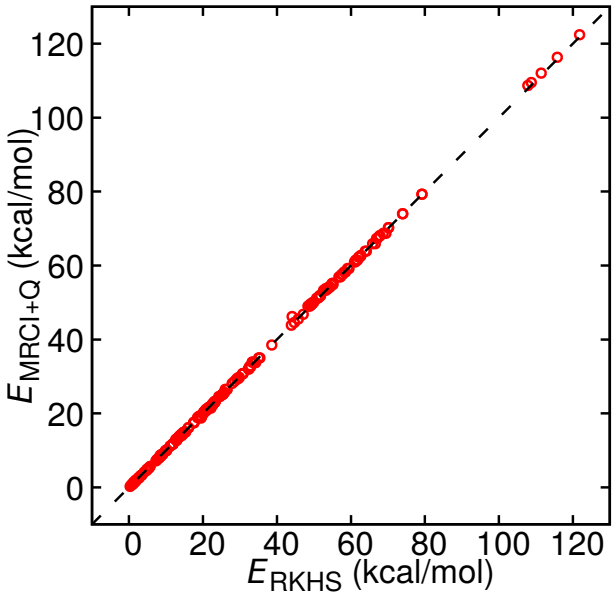

Figure 2: Correlation between the *ab initio* and analytical energies obtained from RKHS interpolation for a set of 245 randomly selected validation points with $R^2 = 0.9999$ and an RMSE of 30 cm^{-1} for energies up to 28.6 kcal/mol (10000 cm^{-1}). The energy of the global minimum is at $E = 0$.

The global minimum of the RKHS PES is the linear N-N-N configuration with two equal N-N bonds of length $r_e = 1.187$ Å. This is in good agreement with the *ab initio* optimized structure (1.189 Å) obtained at the MRCI+Q/aug-cc-pVQZ level of theory in the present

work and with diode laser velocity modulation spectroscopy experiment[27] with a value of 1.188402 Å. In Figure 3 the contour plots of the RKHS PES around the global minimum are shown. The equilibrium bond length from the composite calculations[31] is 1.18461 Å which is somewhat too short.

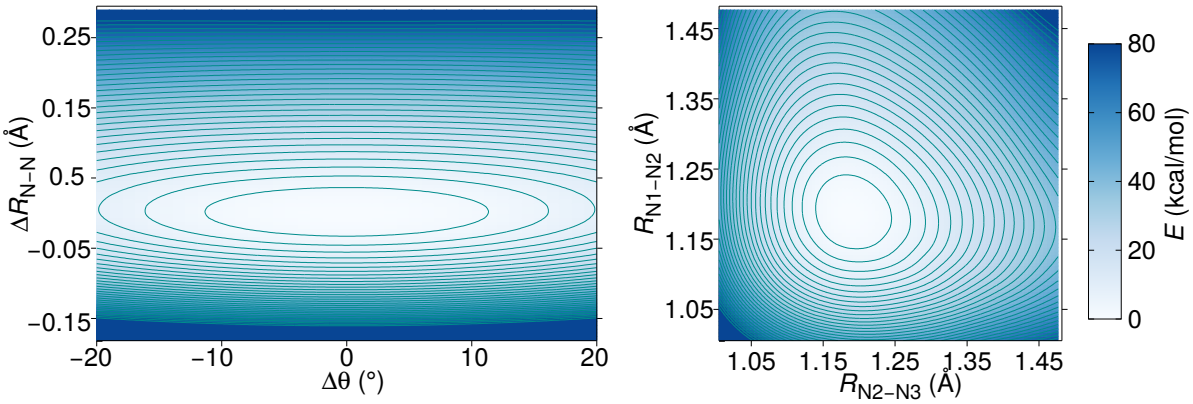

Figure 3: Contour diagrams of the RKHS PES. Left panel: for $R_{\mathrm{N1-N2}} = R_{\mathrm{N2-N3}}$ and $\Delta\theta = 0°$, $\Delta R_{\mathrm{N-N}} = 0$ corresponds to the equilibrium structure. Right panel: for linear N_3^-. The spacing between contours is 2.5 kcal/mol. The zero of energy is the global minimum of the system.

Spectroscopy and Dynamics in the Gas Phase

The quantum bound states for N_3^- were first calculated using DVR3D for $J = 0$ and 1. To validate these results the bound states for $J = 0$ were also determined from time-dependent wave packet calculations. The first 9 bound states for $J = 0$ obtained from both are given in Table S1 in the SI. For the fundamental stretching modes the quantum numbers were assigned upon inspection of the nodal structure of the wave functions, see Figure 4. The transition frequencies for the symmetric (ν_1) and asymmetric (ν_3) stretching mode from DVR3D are 1305.3 and 1973.5 cm^{-1}, respectively, compared with 1305.2 and 1973.4 cm^{-1} from TDQM calculations. Since, N_3^- is linear, the bending fundamental (ν_2) corresponds to a $J = 1$ state and is computed using DVR3D at 632.8 cm^{-1}.

The three fundamental transition frequencies obtained from different methodologies are reported in Table 1 along with the experimentally[27,28,51] and theoretically[31] determined frequencies from the literature. The normal modes shown in Table 1 were calculated using CHARMM together with the RKHS PES. It can be seen that except for the asymmetric stretch, anharmonic and harmonic frequencies agree to within < 5 cm^{-1}. Experimentally, the NN asymmetric stretch in the gas phase was found at 1986.47 cm^{-1} compared with 1973.5 cm^{-1} from the DVR3D calculation[27,28] and 1986.36 cm^{-1} from variational calculations on a parametrized fc-CCSD(T)/aug-cc-pVQZ PES (see Introduction).[31] The difference of ~ 10 cm^{-1} is most likely due to the different level of theory (MRCI vs. composite method based on fc-CCSD(T)) and the smaller basis set used here (aug-cc-pVQZ vs. aug-cc-pV5Z) because the bound state calculations are essentially converged.

To the best of our knowledge, there is no direct experimental data for the bending and symmetric stretching mode in the gas phase. However, infrared and Raman spectra of the azide ion in potassium azide have been determined (642.2 cm^{-1} in KN_3, 642.7 cm^{-1} in KCl cm^{-1}, 640.0 cm^{-1} in KBr, and 638.5 cm^{-1} in KI[51]). These frequencies compare with 632.8 cm^{-1} from quantum calculations. For the symmetric stretch a value of 1344 cm^{-1} was reported[51] in KN_3 somewhat higher, i.e. blue shifted, than 1305.3 cm^{-1} from DVR3D calculations in the gas phase. The variational bound state calculations on the fitted fc-CCSD(T)/aug-cc-pV5Z PES yielded $\nu_2 = 629.3$ cm^{-1}, and $\nu_1 = 1307.9$ cm^{-1}, respectively.[31] All these results agree favourably with the present calculations, see Table 1.

As an independent validation of the bound state calculations, NVE MD simulations with the RKHS-MRCI PES were carried out for N_3^- in the gas phase using CHARMM. Power spectra for the distances r_i (Ni-Nj separation) were determined and compared with results from bound state calculations. Similar analyses were carried out for N_3^- in solution. Moreover, the infrared spectra for N_3^- in water was also calculated from the dipole moment autocorrelation

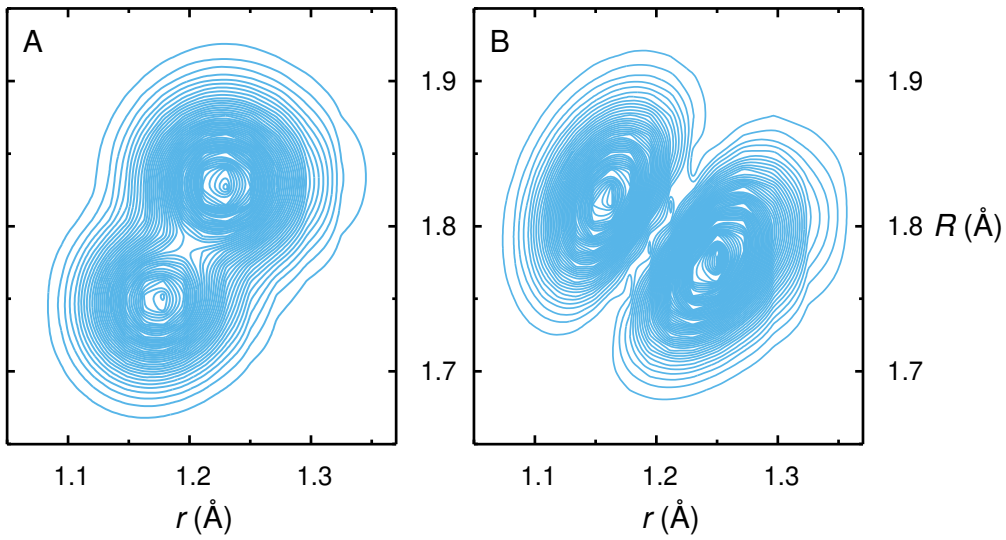

Figure 4: Contour plots of the squared wave function amplitude $|\Psi|^2$ associated with the ν_1 (left) and ν_3 (right) mode from DVR3D calculation on the RKHS PES for N_3^-.

Table 1: Fundamental transition frequencies in cm^{-1} for N_3^-. The frequencies reported in Ref.[31] are obtained from QM calculations on an analytical PES based on CCSD(T)/aug-cc-pV5Z energies.

Mode	Expt.	NMA	DVR3D	TDWP	Power Spec. (300 K)	Ref.[31]
$[1,0,0]$	1344*	1306.8	1305.3	1305.2	1307.4	1307.9
$[0,1,0]$	∼640*	636.6	632.8		637.2	629.3
$[0,0,1]$	1986.47[27,28]	2004.6	1973.5	1973.4	2005.2	1986.4

* Frequencies of N_3^- in potassium halide salts[51]

function.

This suggests that the MD simulations provide a meaningful surrogate for the quantum calculations. Such comparisons are important when considering simulations in solution for which rigorous quantum calculations are not possible and conclusions must be drawn either from MD simulations or from other approximate treatments. For the simulations in solution the maxima of the power spectra shift to $\nu_1 = 1355.4$ cm^{-1}, and $\nu_3 = 2061.9$ cm^{-1} while for 1D-IR spectrum, the peaks are $\nu_2 = 646.8$ cm^{-1}, and $\nu_3 = 2061.1$ cm^{-1}, see Figure 5 and Table 2.

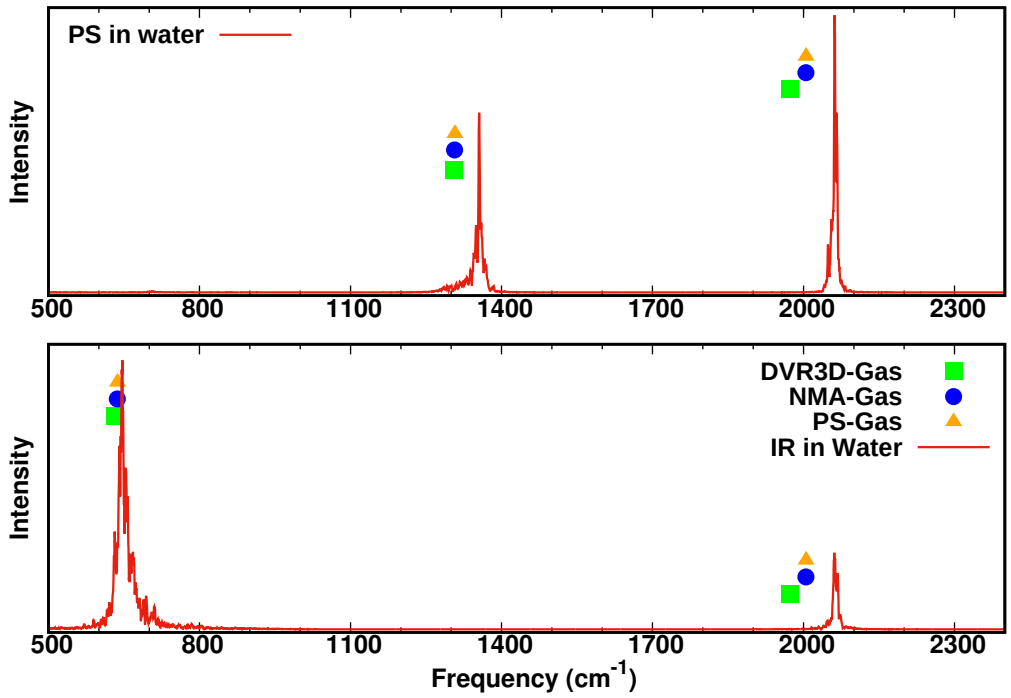

Figure 5: Power and IR spectra for N_3^- in solvent are shown in the upper and lower panel, respectively. The maxima of power ($\nu_1 = 1355.4$ cm^{-1}, and $\nu_3 = 2061.9$ cm^{-1}), IR spectra ($\nu_2 = 646.8$ cm^{-1}, and $\nu_3 = 2061.1$ cm^{-1}) in solvent and the results from DVR3D quantum calculations (green square), the normal mode analysis (blue circle) and the power spectra (orange triangle) all in the gas phase, are shown as well.

Dynamics and Spectroscopy in Solution

To serve as a positionally resolved spectroscopic probe, it is important to characterize the vibrational spectroscopy of N_3^- in solution. The power spectra (see Figure 5) indicate a blue shift of $\Delta\nu_3 = 56.7$ cm^{-1} for the asymmetric stretch. Experimentally, the anti-symmetric stretching mode of the azide ion in bulk water has been found at 2047.5 cm^{-1} which amounts to a blue shift of 61 cm^{-1} for the $[0, 0, 1]$ mode and serves as a comparison for the present simulations.[20] This is also consistent with the situation in CN^- for which the experimentally observed blue shift is 44 cm^{-1} compared with a value of 36 cm^{-1} from atomistic simulations.[14,52,53]

For more rigorous calculations two different analyses for the vibrational dynamics of azide

in solution are considered. One of them uses normal mode calculations for a given solution configuration and the other one recomputes the *effective* 3-dimensional potential energy surface $V(R, r, \theta)$ for a given solvent configuration from which the vibrational states of interest are determined from solving the 3D Schrödinger equation, see Methods.

Table 2: Vibrational Frequencies cm^{-1} for N_3^- in solvent from experiment[20,29] and the present simulations. For the asymmetric stretch fundamental $[0, 0, 1]$ the vibrational blue shift from $P(\omega)$ and the line shape (asterisk) with respect to the gas phase values is also indicated. For INM this is a harmonic shift $\Delta\omega$ and for all other cases it is an anharmonic shift $\Delta\nu$ with respect to the fundamentals in the gas phase, see Table 1.

Mode	Expt	DVR3D	INM	Power Spectrum	IR Spectrum
$[1, 0, 0]$			1327.7	1355.4	
$[0, 1, 0]$			651.2		646.8
$[0, 0, 1]$	2047.5	2038.0	2047.3	2061.9	2061.1
$\Delta\nu_{[0,0,1]}$	61	64	43	57	
		74*	45*		

To determine the peak frequencies of the distributions $P(\omega)$, the raw data was fitted to a log normal probability distribution, see Figure S3. The peak values of $P(\omega)$, are reported in Table 2 along with results obtained from Power and IR spectra and from experiment. The frequency distribution peaks from instantaneous normal modes for the bending, symmetric, and asymmetric stretch are at 651.2 cm^{-1}, 1327.7 cm^{-1}, and 2047.3 cm^{-1}. This compares with the gas phase frequencies using the same analysis at 636.6 cm^{-1}, 1306.8 cm^{-1}, and 2004.6, respectively. From comparing the frequency distributions all modes are shifted to the blue by between 15 cm^{-1} and 43 cm^{-1} (see Table 2). For N_3^- in solution it is expected that $P(\omega)$ deviates somewhat from a Gaussian distribution. Because all fundamentals are shifted to the blue, it is also expected that $P(\omega)$ contains a tail at higher frequencies. This is indeed the case (Figure S3), and the log-normal fits the raw data quite well which indicates that sampling is sufficient and the frequency trajectory is close to converged.

The blue shift from solving the 3-d Schrödinger equation is 64 cm^{-1} (according to $P(\omega)$) and 74 cm^{-1} when considering the IR-lineshape, see Table 2 and Figure 6. This is in reasonable to good agreement with experiment (61 cm^{-1}) and provides a meaningful basis for future applications of the present model in positionally resolved spectroscopy of peptides and proteins in solution. It is also worthwhile to note that the power spectrum, which is readily available from equilibrium MD simulations, yields a meaningful description of the blue shift ($\Delta\nu = 57$ cm^{-1}).

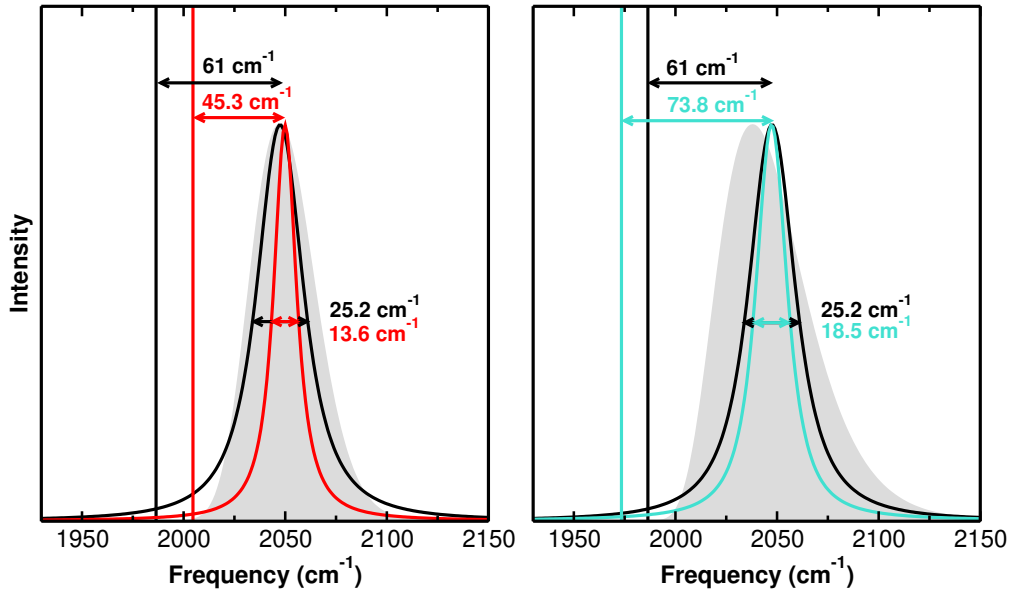

Figure 6: 1D-IR spectrum of N_3^- in water obtained from INM (left panel) and solution of the 3-d Schrödinger equation (3-d SE, right panel) calculations is compared with the FT-IR experiment.[20,27–29] The gas phase frequencies are shown as vertical lines and the remaining traces are experimental lineshapes and those determined from integrating the FFCFs. The black, red and turquoise lines represent experimental, INM and 3-d SE results, respectively. The grey areas indicate the distributions of transition frequencies, $P(\omega)$, for N_3^- in solution from 1.2×10^6 snapshots. The peak frequencies for the 1D-IR spectra from INM and 3-d SE calculations are at 2049.9 cm^{-1} and 2047.3 cm^{-1}, respectively.

In order to characterize the solvent dynamics around N_3^- in solution, the frequency correlation function for the NN asymmetric stretch from INM was determined. The data was fitted to Eq. 6 including three time scales, see Figure 7 and the corresponding fitting pa-

rameters are reported in Table 3. Three time scales can be distinguished in the FFCF: two sub-picosecond time scales ($\tau_1 = 0.044$ ps and $\tau_2 = 0.23$ ps) with large amplitude and one on the picosecond ($\tau_3 = 1.18$ ps) with a smaller amplitude.

Similarly, the FFCF for the asymmetric stretching mode was determined from the same 1.2×10^6 snapshots using DVR3D to solve the 3-dimensional nuclear Schrödinger equation based on scanning the 3-dimensional PES for an instantaneous solvent configuration. The FFCF determined from this time series was again fitted to Eq. 6 using three time scales, see Figure 7B. The corresponding fitting parameters are also reported in Table 3. The three time scales are $\tau_1 = 0.048$ ps, $\tau_2 = 0.21$ ps and $\tau_3 = 1.06$ ps. As for FFCF from INM, τ_3 agrees well with experimental values in D_2O ($\tau = 1.3$ ps)[18] and in H_2O ($\tau \approx 1.2$ ps).[29]

Both FFCFs display a pronounced minimum at very short time ($t \sim 0.1$ ps). This feature is known from previous simulations[50] and related to the strength of the interaction between solvent and solute.[10,14,49] As this interaction is expected to decrease in going from CN^-, N_3^-, H_2O to the amide-I mode in N-methyl-acetamide, the observed behavior in the FFCF is consistent with such an interpretation. A final, less critical[49] characteristic of the FFCF is the amplitude $C(0)$ at zero time of the unnormalized FFCF. Previous simulations[50] found a value of ~ 500 cm^{-1} compared with a value of ~ 275 cm^{-1} from experiment.[18] The FFCF from the instantaneous normal modes and the quantum bound state calculations yield 272 cm^{-1} and 651 cm^{-1}, respectively. On the other hand, it has been found that the experiment is not particularly sensitive to the very short time dynamics[50] as evidenced by the absence of the short-time anticorrelation. It is noted that the general appearance of the FFCF in Figure 7 is comparable to that for CN^- and NMA in water[10,14] and exhibits somewhat larger fluctuations compared with previous simulations of N_3^- in water.[50] This is probably related to the fact in the present case the solute was flexible and the vibrational frequencies for the fundamentals were determined for the instantaneous solvent configurations from solutions of

the 3-d Schrödinger equation whereas the stationary states for CN^- were determined from the analytical formula for bound states of a Morse oscillator,[14] and for NMA in water the chromophore was frozen during the MD simulations[10] which was also the approach followed for azide in water.[50]

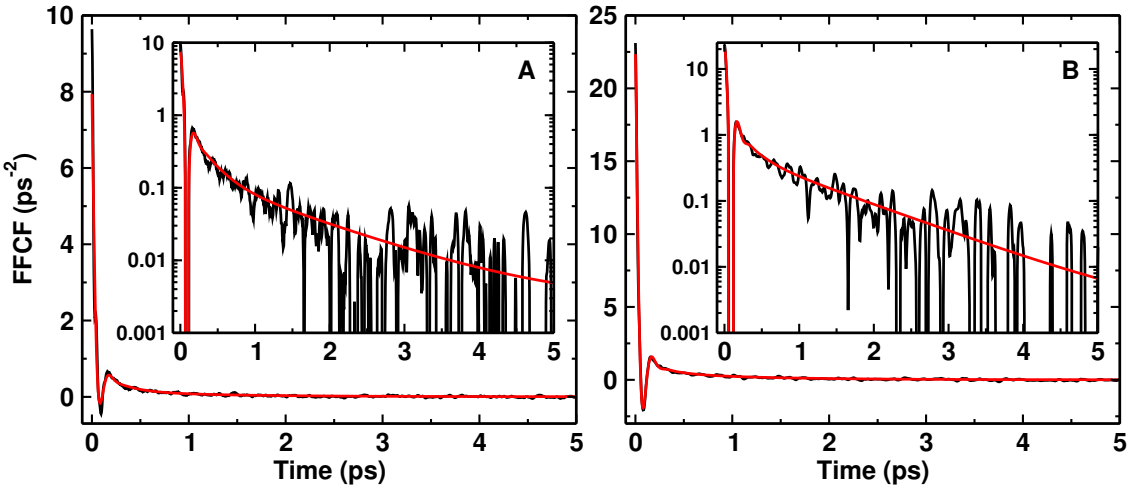

Figure 7: FFCF for the asymmetric stretch vibration as a function of time (black line) from A) INM and B) solution of the 3-dimensional Schrödinger equation for azide in water. Solid red line is the corresponding fit to Eq. 6 with three time scales. The inset shows the same data on a logarithmic scale for the $y-$axis. The rapid initial drop of the FFCF within the first 100 fs (the inertial component[54]) reflects the intermolecular hydrogen bond vibration.

Table 3: Parameters obtained from fitting the FFCF to Eq. 6 for both, frequencies from INM and solutions of the 3-dimensional Schrödinger equation (SE). Average frequency $\langle\omega\rangle$ of the [0,0,1] fundamental in cm^{-1}, the full width at half maximum in cm^{-1}, the amplitudes a_1 to a_3 in ps^{-2}, the decay times τ_1 to τ_3 in ps, the parameter γ in ps^{-1}, and the offset Δ_0 in ps^{-2}. The experimental results in H_2O and in reverse micelles are from Refs.[20,29] and for the decay time in D_2O.[3] Errors, determined from R,[55] for all parameters are given in brackets.

	$\langle\omega\rangle$	FWHM	a_1	a_2	a_3	τ_1	τ_2	τ_3	γ	Δ_0
INM	2049.9	13.6	7.01	0.76	0.16	0.044	0.23	1.18	30.14	0.003
			(0.09)	(0.06)	(0.06)	(0.00)	(0.03)	(0.33)	(0.35)	(0.00)
3-d SE	2047.3	18.5	20.37	1.40	0.57	0.048	0.21	1.06	33.28	0.001
			(0.09)	(0.06)	(0.07)	(0.00)	(0.02)	(0.09)	(0.11)	(0.00)
Expt.	2047.5	25.2						~ 1.2 (H_2O)		
								1.3 (D_2O)		

Figure 6 shows the 1D-IR spectra of the NN asymmetric stretching mode using two different approaches (INM and DVR3D) to compute the frequencies. The observed and computed solvent induced shifts are 45 cm^{-1} and 74 cm^{-1}, respectively, for INM and DVR3D calculations, compared with 61 cm^{-1} from experiment,[20,27,28] see Table 2. They both correctly capture the blue shift but the quantum calculations appear to better describe the 1D-IR spectroscopy. A similar observation is made for the full widths at half maximum (FWHM). Frequencies from instantaneous normal modes yield a FWHM of 13.6 cm^{-1} which increases to 18.5 cm^{-1} when the 3D Schrödinger equation is solved. This compares with 25.2 cm^{-1} from experiment.[20] Hence, the added computational effort in using quantum mechanical frequencies from scanning the 3-dimensional PES for a given solvent configuration indeed provides better results. On the other hand, the considerably more economical approach based on instantaneous normal modes is still a meaningful alternative.

Conclusions

This work introduces an accurate model to characterize the vibrational spectroscopy of N_3^- in solution. Based on a RKHS representation of the intramolecular interactions, the quantum bound states agree well for the fundamentals in the gas phase and in solution as determined from experiment. In particular, for the simulations in water the blue shifts, full widths at half maximum and the time scale of the solvent reorganization dynamics as probed by the asymmetric stretch of N_3^- compare favourably with experiment.

This opens up the possibility to use this model for a spatially sensitive probe of the solvent dynamics in more complex systems, including individual molecules or proteins in solution. Independently, using a suitable flexible, spectroscopically accurate water model such as the Kumagai, Katwamura, Yokokawa (KKY) model[56–58] it will be possible to probe the coupling

between the intramolecular degrees of freedom of solute and solvent as their fundamentals and overtones lead to potentially interesting dynamics. The present model can be further improved by using higher order multipoles[59–62] or polarization[63] to treat the electrostatic interactions. Also, a slight adjustment of the bonded interactions could be envisaged as using stretch and bending potentials from gas phase calculations for simulations in solution is another approximation that is used in the present work. This will be of particular importance when the present model is used for N_3^- as a covalently linked probe to a peptide or a protein residue.

Together with state-of-the art experiments the present work lays the foundation to a molecularly refined picture of the structural dynamics of complex systems in the condensed phase from a combined experimental/simulation approach.

Supporting Information Available

For Table S1, Figures S1 to S3 see supporting information. This material is available free of charge via the Internet at `http://pubs.acs.org/`.

Acknowledgments

This work was supported by the Swiss National Science Foundation, NCCR MUST, and the University of Basel.

References

(1) El Hage, K.; Brickel, S.; Hermelin, S.; Gaulier, G.; Schmidt, C.; Bonacina, L.; van Keulen, S. C.; Bhattacharyya, S.; Chergui, M.; Hamm, P. et al. Implications of Short

Time Scale Dynamics on Long Time Processes. *Struct. Dyn.* **2017**, *4*, 061507.

(2) Koziol, K. L.; Johnson, P. J. M.; Stucki-Buchli, B.; Waldauer, S. A.; Hamm, P. Fast Infrared Spectroscopy of Protein Dynamics: Advancing Sensitivity and Selectivity. *Curr. Op. Struct. Biol.* **2015**, *34*, 1–6.

(3) Hamm, P.; Lim, M.; Hochstrasser, R. M. Structure of the Amide I Band of Peptides Measured by Femtosecond Nonlinear-Infrared Spectroscopy. *J. Phys. Chem. B* **1998**, *5647*, 6123–6138.

(4) Hamm, P.; Zanni, M. *Concepts and Methods of 2D Infrared Spectroscopy*; Cambridge University Press: New York, 2011.

(5) Zanni, M. T.; Asplund, M. C.; Hochstrasser, R. Two-Dimensional Heterodyned and Stimulated Infrared Photon Echoes of N-methylacetamide-D. *J. Chem. Phys.* **2001**, *114*, 4579–4590.

(6) Hamm, P.; Hochstrasser, R. M. In *Ultrafast Infrared and Raman Spectroscopy*; Fayer, M. D., Ed.; Marcel Dekker: New York, 2001; pp 273–347.

(7) DeCamp, M. F.; DeFlores, L.; McCracken, J. M.; Tokmakoff, A.; Kwac, K.; Cho, M. Amide I Vibrational Dynamics of N-Methylacetamide in Polar Solvents: The Role of Electrostatic Interactions. *J. Phys. Chem. B* **2005**, *109*, 11016–11026.

(8) Bastida, A.; Soler, M. A.; Zuniga, J.; Requena, A.; Kalstein, A.; Fernandez-Alberti, S. Instantaneous Normal Modes, Resonances, and Decay Channels in the Vibrational Relaxation of the Amide I Mode of N-methylacetamide-D in Liquid Deuterated Water. *J. Chem. Phys.* **2010**, *132*, 224501.

(9) Bastida, A.; Soler, M. A.; Zuniga, J.; Requena, A.; Kalstein, A.; Fernandez-Alberti, S. Hybrid Quantum/Classical Simulations of the Vibrational Relaxation of the Amide I Mode of N-Methylacetamide in D_2O Solution. *J. Phys. Chem. B* **2012**, *116*, 2969–2980.

(10) Cazade, P.-A.; Bereau, T.; Meuwly, M. Computational Two-Dimensional Infrared Spectroscopy without Maps: N-Methylacetamide in Water. *J. Phys. Chem. B* **2014**, *118*, 8135–8147.

(11) Rey, R.; Hynes, J. T. Vibrational Phase and Energy Relaxation of CN^- in water. *J. Chem. Phys.* **1998**, 142–153.

(12) Lee, M. W.; Meuwly, M. On the Role of Nonbonded Interactions in Vibrational Energy Relaxation of Cyanide in Water. *J. Phys. Chem. A* **2011**, *115*, 5053–5061.

(13) Koziński, M.; Garrett-Roe, S.; Hamm, P. Vibrational Spectral Diffusion of CN^- in Water. *Chem. Phys.* **2007**, *341*, 5–10.

(14) Lee, M. W.; Carr, J. K.; Göllner, M.; Hamm, P.; Meuwly, M. 2D IR Spectra of Cyanide in Water Investigated by Molecular Dynamics Simulations. *J. Chem. Phys.* **2013**, *139*, 054506.

(15) Suydam, I. T.; Snow, C. D.; Pande, V. S.; Boxer, S. G. Electric Fields at the Active Site of an Enzyme : Direct Comparison of Experiment with Theory. *Science* **2006**, *313*, 200–204.

(16) Mondal, P.; Meuwly, M. Vibrational Stark Spectroscopy for Assessing Ligand-Binding Strengths in a Protein. *Phys. Chem. Chem. Phys.* **2017**, *19*, 16131–16143.

(17) Li, M.; Owrutsky, J.; Sarisky, M.; Culver, J. P.; Yodh, A.; Hochstrasser, R. M. Vibrational and Rotational Relaxation-Times of Solvated Molecular-Ions. *J. Chem. Phys.* **1993**, *98*, 5499–5507.

(18) Hamm, P.; Lim, M.; Hochstrasser, R. Non-Markovian Dynamics of the Vibrations of Ions in Water from Femtosecond Infrared Three-Pulse Photon Echoes. *Phys. Rev. Lett.* **1998**, *81*, 5326–5329.

(19) Zhong, Q.; Baronavski, A.; Owrutsky, J. Vibrational Energy Relaxation of Aqueous Azide Ion Confined in Reverse Micelles. *J. Chem. Phys.* **2003**, *118*, 7074–7080.

(20) Maekawa, H.; Ohta, K.; Tominaga, K. Spectral Diffusion of the Anti-Symmetric Stretching Mode of Azide Ion in a Reverse Micelle Studied by Infrared Three-Pulse Photon Echo Method. *Phys. Chem. Chem. Phys.* **2004**, *6*, 4074–4077.

(21) Li, S.; Schmidt, J. R.; Skinner, J. L. Vibrational Energy Relaxation of Azide in Water. *J. Chem. Phys.* **2006**, *125*, 244507.

(22) Li, S.; Lawrence, C.; Skinner, J. Vibrational Spectral Diffusion of Azide Anion in Water. *Abstr. Pap. Am. Chem. Soc.* **2005**, *229*, U775.

(23) Choi, J.-H.; Raleigh, D.; Cho, M. Azido Homoalanine is a Useful Infrared Probe for Monitoring Local Electrostatistics and Side-Chain Solvation in Proteins. *J. Phys. Chem. Lett.* **2011**, *2*, 2158–2162.

(24) Borek, J.; Perakis, F.; Klaesi, F.; Garrett-Roe, S.; Hamm, P. Azide-Water Intermolecular Coupling Measured by Two-Color Two-Dimensional Infrared Spectroscopy. *J. Chem. Phys.* **2012**, *136*.

(25) Ohta, K.; Tayama, J.; Tominaga, K. Ultrafast Vibrational Dynamics of SCN^- and N_3^- in Polar Solvents Studied by Nonlinear Infrared Spectroscopy. *Phys. Chem. Chem. Phys.* **2012**, *14*, 10455–10465.

(26) Zhong, Q.; Baronavski, A.; Owrutsky, J. Reorientation and Vibrational Energy Relaxation of Pseudohalide Ions Confined in Reverse Micelle Water Pools. *J. Chem. Phys.* **2003**, *119*, 9171–9177.

(27) Polak, M.; Gruebele, M.; Saykally,; Kaldor, R. Velocity Modulation Laser Spectroscopy of Negative Ions: The ν_3 Band of Azide (N_3^-). *J. Am. Chem. Soc.* **1987**, *109*, 2884–2887.

(28) Polak, M.; Gruebele, M.; Peng, G.; Saykally, R. Velocity Modulation Infrared Laser Spectroscopy of Negative Ions: The (011)-(001) Band of Azide (N_3^-). *J. Chem. Phys.* **1988**, *89*, 110–114.

(29) Maekawa, H.; Ohta, K.; Tominaga, K. Vibrational Dynamics in Liquids Studied by Non-linear Infrared Spectroscopy. *Res. Chem. Intermed.* **2005**, *31*, 703–716.

(30) Garcia-Viloca, M.; Nam, K.; Alhambra, C.; Gao, J. Solvent and Protein Effects on the Vibrational Frequency Shift and Energy Relaxation of the Azide Ligand in Carbonic Anhydrase. *J. Phys. Chem. B* **2004**, *108*, 13501–13512.

(31) Sebald, P.; Stein, C.; Oswald, R.; Botschwina, P. Rovibrational States of N_3^- and CO_2 Up to High J: A Theoretical Study Beyond fc-CCSD(T). *J. Phys. Chem. A* **2013**, *117*, 13806–13814.

(32) Werner, H.-J.; Knowles, P. J.; Knizia, G.; Manby, F. R.; Schütz, M. Molpro: A General-Purpose Quantum Chemistry Program Package. *WIREs Comput. Mol. Sci.* **2012**, *2*, 242–253.

(33) Werner, H.-J.; Knowles, P. J.; Knizia, G.; Manby, F. R.; Schütz, M.; Celani, P.; Györffy, W.; Kats, D.; Korona, T.; Lindh, R. et al. MOLPRO, Version 2012.1, A Package of ab Initio Programs. 2012.

(34) Meuwly, M.; Hutson, J. The Potential Energy Surface and Near-dissociation States of He-H_2^+. *J. Chem. Phys.* **1999**, *110*, 3418–3427.

(35) Ho, T.-S.; Rabitz, R. A General Method for Constructing Multidimensional Molecular Potential Energy Surfaces from ab Initio Calculations. *J. Chem. Phys.* **1996**, *104*, 2584–2597.

(36) Unke, O. T.; Meuwly, M. Toolkit for the Construction of Reproducing Kernel-Based

Representations of Data: Application to Multidimensional Potential Energy Surfaces. *J. Chem. Inf. Model.* **2017**, *57*, 1923–1931.

(37) Hollebeek, T.; Ho, T.-S.; Rabitz, H. Constructing Multidimensional Molecular Potential Energy Surfaces from ab Initio Data. *Ann. Rev. Phys. Chem.* **1999**, *50*, 537–570.

(38) Tennyson, J.; Kostin, M. A.; Barletta, P.; Harris, G. J.; Polyansky, O. L.; Ramanlal, J.; Zobov, N. F. DVR3D: A Program Suite for the Calculation of Rotation-Vibration Spectra of Triatomic Molecules. *Comp. Phys. Comm.* **2004**, *163*, 85–116.

(39) Sutcliffe, B.; Tennyson, J. A General Treatment of Vibration-Rotation Coordinates for Triatomic Molecules. *Int. J. Quant. Chem.* **1991**, *39*, 183–196.

(40) Koner, D.; Barrios, L.; González-Lezana, T.; Panda, A. N. Scattering Study of the Ne + $NeH^+(v_0 = 0, j_0 = 0) \rightarrow NeH^+$ + Ne Reaction on an ab Initio Based Analytical Potential Energy Surface. *J. Chem. Phys.* **2016**, *144*, 034303.

(41) Feit, M. D.; J. A. Fleck, J.; Steiger, A. Solution of the Schödinger Equation by a Spectral Method. *J. Comp. Phys.* **1982**, *47*, 412–433.

(42) Brooks, B. R.; Brooks III, C. L.; MacKerell Jr., A. D.; Nilsson, L.; Petrella, R. J.; Roux, B.; Won, Y.; Archontis, G.; Bartels, C.; Boresch, S. et al. CHARMM: The Biomolecular Simulation Program. *J. Comp. Chem.* **2009**, *30*, 1545–1614.

(43) Jorgensen, W. L.; Chandrasekhar, J.; Madura, J. D.; Impey, R. W.; Klein, M. L. Comparison of Simple Potential Functions for Simulating Liquid Water. *J. Chem. Phys.* **1983**, *79*, 926–935.

(44) Gunsteren, W. V.; Berendsen, H. Algorithms for Macromolecular Dynamics and Constraint Dynamics. *Mol. Phys.* **1997**, *34*, 1311–1327.

(45) Morita, A.; Kato, S. Vibrational Relaxation of Azide Ion in Water: The Role of Intramolecular Charge Fluctuation and Solvent-Induced Vibrational Coupling. *J. Chem. Phys.* **1998**, *109*, 5511–5523.

(46) Cazade, P.-A.; Bereau, T.; Meuwly, M. Computational Two-Dimensional Infrared Spectroscopy without Maps: N-Methylacetamide in Water. *J. Phys. Chem. B* **2014**, *118*, 8135–8147.

(47) Hedin, F.; El Hage, K.; Meuwly, M. A Toolkit to Fit Nonbonded Parameters from and for Condensed Phase Simulations. *J. Chem. Theo. Comp.* **2016**, *56*, 1479–1489.

(48) Hedin, F.; El Hage, K.; Meuwly, M. A Toolkit to Fit Nonbonded Parameters from and for Condensed Phase Simulations (vol 56, pg 1479, 2016). *J. Chem. Theo. Comp.* **2017**, *57*, 102–103.

(49) Moller, K.; Rey, R.; Hynes, J. Hydrogen Bond Dynamics in Water and Ultrafast Infrared Spectroscopy: A Theoretical Study. *J. Phys. Chem. A* **2004**, *108*, 1275–1289.

(50) Li, S.; Schmidt, J. R.; Piryatinski, A.; Lawrence, C. P.; Skinner, J. L. Vibrational Spectral Diffusion of Azide in Water. *J. Phys. Chem. B* **2006**, *110*, 18933–18938.

(51) Lamoureux, R.; Dows, D. Infrared and Raman Spectra of Azide Ion in Potassium Azide and Potassium Halides. *Spectroc. Acta Pt. A-Molec. Biomolec. Spectr.* **1975**, *31*, 1945–1949.

(52) Bradforth, S. E.; Kim, E. H.; Arnold, D. W.; Neumark, D. M. Photoelectron Spectroscopy of CN^-, NCO^-, and NCS^-. *J. Chem. Phys.* **1993**, *98*, 800–810.

(53) Hamm, P.; Lim, M.; Hochstrasser, R. M. Vibrational Energy Relaxation of the Cyanide ion in Water. *J. Chem. Phys.* **1997**, *107*, 10523–10531.

(54) Laage, D.; Stirnemann, G.; Sterpone, F.; Rey, R.; Hynes, J. T. Reorientation and

Allied Dynamics in Water and Aqueous Solutions. *Annu. Rev. Phys. Chem.* **2011**, *62*, 395–416.

(55) R Core Team, R: A Language and Environment for Statistical Computing. R Foundation for Statistical Computing: Vienna, Austria, 2013.

(56) Kumagai, N.; Kawamura, K.; Yokokawa, T. An Interatomic Potential Model for H_2O: Applications to Water and Ice Polymorphs. *Mol. Sim.* **1994**, *12*, 177–186.

(57) Plattner, N.; Meuwly, M. Atomistic Simulations of CO Vibrations in Ices Relevant to Astrochemistry. *ChemPhysChem* **2008**, *9*, 1271–1277.

(58) Pezzella, M.; Unke, O. T.; Meuwly, M. Molecular Oxygen Formation in Interstellar Ices Does Not Require Tunneling. *J. Phys. Chem. Lett.* **2018**, *9*, 1822–1826.

(59) Plattner, N.; Meuwly, M. The Role of Higher CO-Multipole Moments in Understanding the Dynamics of Photodissociated Carbonmonoxide in Myoglobin. *Biophys. J.* **2008**, *94*, 2505–2515.

(60) Devereux, M.; Plattner, N.; Meuwly, M. Application of Multipolar Charge Models and Molecular Dynamics Simulations to Study Stark Shifts in Inhomogeneous Electric Fields. *J. Phys. Chem. A* **2009**, *113*, 13199–13209.

(61) Bereau, T.; Kramer, C.; Meuwly, M. Leveraging Symmetries of Static Atomic Multipole Electrostatics in Molecular Dynamics Simulations. *J. Chem. Theo. Comp.* **2013**, *9*, 5450–5459.

(62) El Hage, K.; Gupta, P. K.; Bemish, R.; Meuwly, M. Molecular Mechanisms Underlying Solute Retention at Heterogeneous Interfaces. *J. Phys. Chem. Lett.* **2017**, *8*, 4600–4607.

(63) Anisimov, V.; Lamoureux, G.; Vorobyov, I.; Huang, N.; Roux, B.; MacKerell, A. Determination of Electrostatic Parameters for a Polarizable Force Field Based on the Classical Drude Oscillator. *J. Chem. Theo. Comp.* **2005**, *1*, 153–168.